

On Perpendicular Texture

or: Why do we see more flowers in the distance?

Thomas Leung and Jitendra Malik

Computer Science Division, University of California at Berkeley
Berkeley, CA 94720
{leungt,malik}@cs.berkeley.edu

Abstract

Almost all work on texture in the computer vision and graphics communities has modeled the texture as tangential, i.e. lying in the tangent plane to the surface. This is equivalent to thinking of the texture as a pattern painted on the surface. Three-dimensional textures, where the elements may point out of the surface, have largely been ignored. We study a special class of 3D textures, perpendicular textures where we can model the elements as being normal to the surface. The perspective projection of perpendicularly textured surfaces results in several interesting phenomena, which do not occur in the much-studied tangential texture case. These include occlusion, foreshortening and illumination.

In this paper, we study the geometry of the problem, modeling the locations of the elements of the texture as being a realization of a spatial point process. Relations between slant and tilt of the surface, density and height of elements and occlusions are derived. Occlusions can now be used as a cue to infer shape, instead of being treated as a source of error.

1 Introduction

Almost all work on texture in the computer vision and graphics communities has modeled the texture as tangential, i.e. lying in the tangent plane to the surface [1, 2, 3, 4, 5, 8].¹ This is equivalent to thinking of the texture as a pattern painted on the surface. Spots on a leopard, or the stripes on a zebra are canonical examples. Three-dimensional textures, where the elements may point out of the surface, have largely been ignored. However, such textures e.g. animal fur, hair, fields of yellow flowers are in fact quite common in our visual world. Some examples are shown in Figure 1. We study a special class of 3D textures, *perpendicular* textures where we can model the elements as being normal to the surface. The perspective projection of perpendicularly textured surfaces results in several interesting phenomena, which do not occur in the much-studied tangential texture case. These include (1) Occlusion: When an element is behind another one in the line of sight, part of it will be occluded. This problem is aggravated when the orientation of the surface

¹Despite the tangential texture assumption, [2] managed to recover reasonable shape information for 3D textures by detecting texels and restricting to planar surfaces. However, occlusion is treated as error which has to be dealt with.

changes, causing different parts of the elements to be seen. (2) Foreshortening: The relation of foreshortening to slant and tilt is different for tangential and perpendicular textures. (3) Illumination: Elements no longer lie on a surface, therefore, self-shadowing has to be considered.

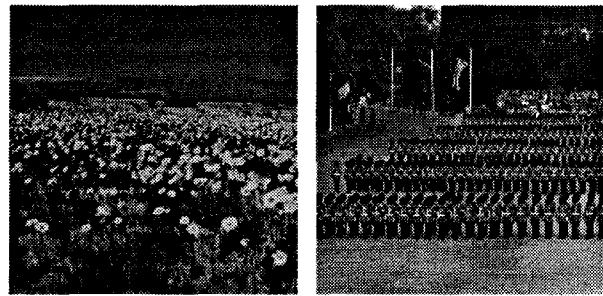


Figure 1: Some examples of perpendicular texture.

In this paper, we study (1) – the occlusion properties of perpendicular texture. We model the locations of the elements of the texture as being a realization of a spatial point process. Relations between slant and tilt of the surface, density, height and radius of elements and occlusions are derived. Occlusions can now be used as a cue to infer shape, instead of being treated as a source of error. Of the other two problems in the study of perpendicular textures, (2) remains largely unexplored; (3) was considered by Koenderink and van Doorn in their work on the photometry of meso structure on surfaces in [7].

The most related work is by Kajiyama and Kay [6], where they studied the problem of rendering fur. They used a volume of “particles” to model the properties of fur. Rendering is basically calculating the amount of light transmitted and attenuated when passing through the volume.

2 Texture Model

We model the locations of the elements of the texture as being a realization of a spatial point process (also known as a point field). The simplest example is the homogeneous Poisson field, which assumes that (1) the number of points in a window is a Poisson random variable; (2) the numbers of points in two disjoint windows are independent. The Poisson field is usually

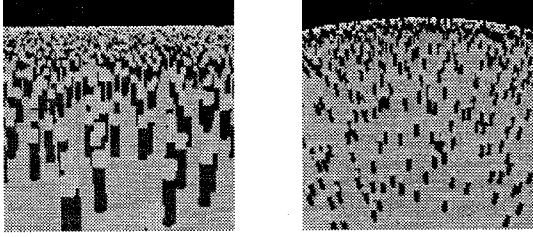


Figure 2: Realizations of our model on planar and curved surfaces.

perceived as a completely random point field. Another interesting example is the hard core model, where the elements are prohibited to lie within a certain inhibition radius from each other. For more details about spatial point processes, the reader is referred to [9, 10].

We model the elements as identical cylinders (radius r , height h) pointing out of the surface. The color/albedo of an element may change along its vertical extent. Figure 2 are two realizations of our model, one for a planar surface, and one for a curved surface.

3 Viewing Geometry

The basic geometry is shown in Figure 3. Our notations follow that of Gårding [4]. The viewer is looking at a smooth surface S projected onto the image sphere Σ . The backprojection map F from Σ to S is defined by $F(\mathbf{p}) = \mathbf{r}(\mathbf{p}) = r(\mathbf{p})\mathbf{p}$, where \mathbf{p} is a unit vector from the focal point to a point on the image sphere, and $r(\mathbf{p})$ is the distance along the visual ray from the focal point through \mathbf{p} to the corresponding point $\mathbf{r} = F(\mathbf{p})$ on the surface S . The differential of the backprojection map F_* maps tangent vectors of Σ at \mathbf{p} to tangent vectors of S at $F(\mathbf{p})$.

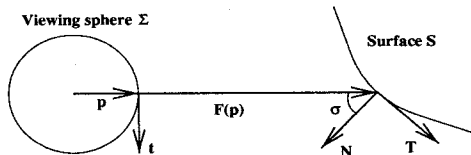


Figure 3: Local surface geometry.

Define the tilt direction \mathbf{t} in $T_{\mathbf{p}}(\Sigma)$, the tangent plane of the viewing sphere at \mathbf{p} , to be a unit vector in the direction of the gradient of the distance function $r(\mathbf{p})$, and the auxiliary vector $\mathbf{b} = \mathbf{p} \times \mathbf{t}$. Then (\mathbf{t}, \mathbf{b}) form an orthonormal basis for the tangent plane to the image sphere Σ and together with \mathbf{p} constitute an orthonormal frame field on Σ . Gårding shows that \mathbf{t} and \mathbf{b} backproject to orthogonal vectors $F_*(\mathbf{t}) = r'\mathbf{p} + r\mathbf{t}$ and $F_*(\mathbf{b}) = r\mathbf{b}$ in the tangent space $T_{F(\mathbf{p})}(S)$, where r' is the directional derivative of the distance r with respect to \mathbf{t} . Defining $\mathbf{T} = F_*(\mathbf{t})/|F_*(\mathbf{t})|$ and $\mathbf{B} = -F_*(\mathbf{b})/|F_*(\mathbf{b})|$ gives us an orthonormal basis (\mathbf{T}, \mathbf{B}) of the tangent space of the surface at $F(\mathbf{p})$. The vectors \mathbf{T}, \mathbf{B} along with the unit normal to the surface $\mathbf{N} = \mathbf{T} \times \mathbf{B}$ constitute

an orthonormal frame field on the surface. The slant angle σ is defined to be the angle between the surface normal \mathbf{N} and the viewing direction \mathbf{p} , so that $\cos \sigma = -\mathbf{N} \cdot \mathbf{p}$. One important point to notice is that \mathbf{b} and \mathbf{B} are parallel. This implies that \mathbf{p}, \mathbf{N} and \mathbf{T} lie on the same plane. This is the plane of normal section due to \mathbf{T} . We call this plane $\mathcal{P}_{\mathbf{T}}$. From the point of view of occlusion, what happens on $\mathcal{P}_{\mathbf{T}}$ is all we have to care about. The reason is that the viewing direction \mathbf{p} lies on $\mathcal{P}_{\mathbf{T}}$ and occlusion can happen only when an object is along the viewing direction.

4 Planar Surfaces

We first consider planar surfaces. One nice fact about planar surfaces is that the surface normal is everywhere parallel to $\mathcal{P}_{\mathbf{T}}$. This implies that either a surface normal lies completely on $\mathcal{P}_{\mathbf{T}}$, or it does not intersect $\mathcal{P}_{\mathbf{T}}$ at all. In other words, assuming that each element is infinitesimally thin, no element will intersect the viewing ray unless it lies on $\mathcal{P}_{\mathbf{T}}$.

4.1 Occlusion Properties

We first calculate the probability that a certain element will be occluded. Imagine looking at the surface at a slant of σ in Figure 2 (a). The side and top views of the situation are shown in Figure 4. The elements are of constant height h and radius r . y_i is a normalized measure along the vertical extent of the element and goes from 0 to 1. The frame field $(\mathbf{T}, \mathbf{B}, \mathbf{N})$ discussed in Section 3 is defined at the point where the viewing ray hits the surface. It is used as the local coordinate system.

Occlusions happen only when an element intersects the viewing ray. The locations on the surface at which surface normals of height h intersect the viewing ray is a curve. We call this curve the *base curve* C_b . C_b is a straight line segment for a planar surface, as shown in Figure 4. By simple geometry, the length of the base curve $l(C_b)$ is $h \tan \sigma$. Taking into account the radius of each element, the locations on the surface at which elements can intersect the viewing ray is well-approximated by a *tube* of width $2r$ along C_b . We call this tube the *base region* R_b .

What we see in a particular viewing direction can be expressed very simply using the base curve. Consider the middle element in Figure 4. We will be able to see it if there are no elements lying in the region R_2 , which is a *tube* of width $2r$ along the appropriate part of C_b . Therefore, the probability that this element will not be occluded is just the probability that no element lies in the region R_2 . The answer is very simple if the locations of the elements follow a homogeneous Poisson field.² For a poisson field model, the number of elements in a window W is a poisson random variable with parameter $\lambda A(W)$, where $A(W)$ is the area of W . λ is called the intensity of the point field, which is the expected number of elements inside

²Note that the Poisson model can be used only as an approximation – cylinders of radius r cannot be placed less than $2r$ apart. A hard core model with inhibition radius r would be more accurate. However, for mathematical tractability, we prefer to use the Poisson model and remark that this is a valid approximation for textures that are relatively sparse ($\lambda \pi r^2 \ll 1$).

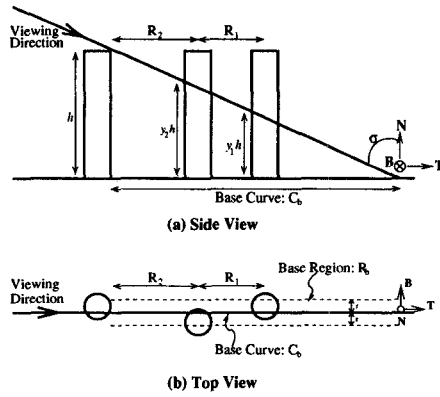


Figure 4: Side and top views of the viewing geometry for elements lying on a plane. In the side view, the page is the \mathcal{P}_T plane. The locations on the surface at which surface normals of height h intersect the viewing ray define the *base curve* C_b .

a region of unit area. Therefore, the probability that no elements appear in W is $\exp(-\lambda A(W))$. The area of R_2 is $2r(1 - y_2)h \tan \sigma$ and so the probability of no occlusion is:

$$\begin{aligned} P_{NO} &= \Pr(N(R_2) = 0) \\ &= \exp(-2\lambda hr(1 - y_2) \tan \sigma) \end{aligned} \quad (1)$$

where $N(W)$ denotes the number of elements in the region W .

We can decompose the exponent of P_{NO} into the product of three terms: $-2\lambda hr \cdot (1 - y) \cdot \tan \sigma$, each with a simple physical interpretation:

1. λhr is a dimensionless constant which is a measure of the “crowdedness” of the texture. It increases with density λ (no. of elements m^{-2}), height h (m), and radius r (m). As “crowdedness” increases ($\lambda hr \uparrow$), P_{NO} decreases. This is a very intuitive relation. Imagine standing in the middle of Manhattan, all the buildings around you are tall and close to each other. The probability of seeing the sun is very low. When buildings get taller ($h \uparrow$), or denser ($\lambda \uparrow$), or wider ($r \uparrow$), the probability of seeing the sun becomes even lower.
2. P_{NO} decreases as $\exp(-\tan \sigma)$. When one looks at the surface at grazing angles (σ tends to 90°), the probability of seeing the element at height yh tends to 0. Conversely, perpendicular texture becomes like tangential texture as $\sigma \rightarrow 0$. In Manhattan, it’s more likely to see the sun at noon than at sunset.
3. P_{NO} increases as y increases, meaning the base of the element is more likely to be occluded than the tip, or intuitively: The higher you are in a building, the more likely you will see the sun.

Equation 1 tells us the visibility probability, conditional on the existence of an element that we are

looking at. In an image, however, what we observe at a certain pixel is the color or the gray-scale value. So the natural question to ask is: what is the probability of seeing a particular color, say yellow, which is painted on the element from the height $y_1 h$ to $y_2 h$? Again, the answer is very simple. It is the probability that at least one element lies in the region R_1 and no element lies in region R_2 of Figure 4:

$$\begin{aligned} \Pr(\text{yellow}) &= \Pr(N(R_2) = 0) \cdot \Pr(N(R_1) > 0) \\ &= e^{-\lambda A(R_2)} \cdot (1 - e^{-\lambda A(R_1)}) \\ &= e^{-2\lambda hr(1 - y_2) \tan \sigma} - e^{-2\lambda hr(1 - y_1) \tan \sigma} \end{aligned} \quad (2)$$

where we used $A(R_1) = \exp(-2\lambda hr(y_2 - y_1) \tan \sigma)$ and $A(R_2) = \exp(-2\lambda hr(1 - y_2) \tan \sigma)$.

The probability of seeing the top of the elements is the area occupied by the element versus the total area: $\lambda \pi r^2$. This holds only when $\sigma < 90^\circ$. Also, recall that we have used a poisson model in the above calculations. It is applicable only when $\lambda \pi r^2 \ll 1$ meaning that the area occupied by the elements is small compared to the total area. Therefore, the probability of seeing the top can usually be ignored.

4.2 “Field of Yellow Flowers”

Let us consider an example of a field of yellow flowers (Figure 1). We model it by cylinders distributed on the plane according to a homogeneous Poisson field. The lower 3/4 of the stem is green, while the upper 1/4 of the stem and the top of the flower is yellow. Using Equation 2, the probabilities are:

$$\Pr(\text{green}) = e^{-\frac{1}{2}\lambda hr \tan \sigma} - e^{-2\lambda hr \tan \sigma} \quad (3)$$

$$\Pr(\text{yellow}) = 1 - e^{-\frac{1}{2}\lambda hr \tan \sigma} + \lambda \pi r^2 \quad (4)$$

$$\begin{aligned} \Pr(\text{ground}) &= 1 - \Pr(\text{green}) - \Pr(\text{yellow}) \\ &= e^{-2\lambda hr \tan \sigma} - \lambda \pi r^2 \end{aligned} \quad (5)$$

The probabilities are plotted as the solid curves in Figure 10(a). At small slant angles, we are more likely to see green than yellow. However, when slant is approaching 90° , we basically just see yellow. Thus we answer the question in the title of the paper: Why do we see more flowers in the distance?

5 Curved Surfaces

One fact we exploited in our study of planar surfaces is that the elements are parallel to each other and to \mathcal{P}_T ; however, this is not true for curved surfaces. Elements lying outside \mathcal{P}_T can intersect the viewing ray, thus cause occlusion. Figure 5 shows a cylindrical surface. The viewing direction is 30° from the axis of the cylinder. Surface normals on the side of the cylinder can intersect \mathcal{P}_T , the (T, N) plane.

Consider the local frame field (T, B, N) , the change in the surface normal is given by the *shape operator*:

$$\begin{bmatrix} -\nabla_T N \\ -\nabla_B N \end{bmatrix} = \begin{bmatrix} \kappa_t & \tau \\ \tau & \kappa_b \end{bmatrix} \begin{bmatrix} T \\ N \end{bmatrix}$$

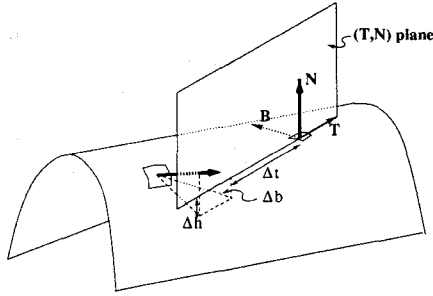


Figure 5: A cylindrical surface. The viewing direction is 30° from the axis of the cylinder. Surface normals on the side of the cylinder can intersect the (\mathbf{T}, \mathbf{N}) plane. A general formula for the intersection point will be derived in Section 5.1.2.

where κ_t and κ_b are the normal curvatures in the \mathbf{T} and \mathbf{B} directions respectively and τ is the geodesic torsion. We adopt the convention that curvature is negative for convex surfaces. By linearity, for any vector $\mathbf{v} = \Delta t \mathbf{T} + \Delta b \mathbf{B}$, the change in surface normal is:

$$\nabla_{\mathbf{v}} \mathbf{N} = -(\Delta t \kappa_t + \Delta b \tau) \mathbf{T} - (\Delta t \tau + \Delta b \kappa_b) \mathbf{B} \quad (6)$$

$\delta_t = -(\Delta t \kappa_t + \Delta b \tau)$ represents a rotation of the surface normal along \mathbf{T} and $\delta_b = -(\Delta t \tau + \Delta b \kappa_b)$ a rotation along \mathbf{B} .

5.1 Occlusion Properties

In this paper, we study the occlusion properties locally. For general curved objects, a local study is not adequate. However, if the surface satisfies certain assumptions, a local study is enough. (1) We assume there is no long-range effect on occlusion. This is generally true for globally convex objects, ie. $\kappa_t < 0$ and $\kappa_b < 0$ everywhere. (2) The texture elements are *small* compared to the global structure. This implies $|h\kappa| \ll 1$ where κ is one of the curvature parameters $(\kappa_t, \kappa_b, \tau)$.

As in the planar case, we want to compute the base curve on which surface normals of height h will intersect the viewing ray. In the general case, surface normals lying outside the (\mathbf{T}, \mathbf{N}) plane can intersect the viewing ray, thus the base curve does not lie completely on the (\mathbf{T}, \mathbf{N}) plane.

5.1.1 Principal Viewing Directions

We first consider the special case $\tau = 0$. This corresponds to looking at the surface from one of the two local principal curvature directions. For a cylinder, a principal curvature direction is along the axis or perpendicular to it; for a sphere or a plane, it is any direction. When $\tau = 0$, Equation 6 can be rewritten as $\nabla_{\mathbf{v}} \mathbf{N} = -\Delta t \kappa_t \mathbf{T} - \Delta b \kappa_b \mathbf{B}$. If the surface is locally convex, $\kappa_b < 0$. Thus the rotation along \mathbf{B} ($\delta_b = -\Delta b \kappa_b$) has the same sign as Δb . What this means is that the surface normal is rotated away from the (\mathbf{T}, \mathbf{N}) plane. Therefore, when $\Delta b \neq 0$, the surface normal will never intersect the viewing ray,

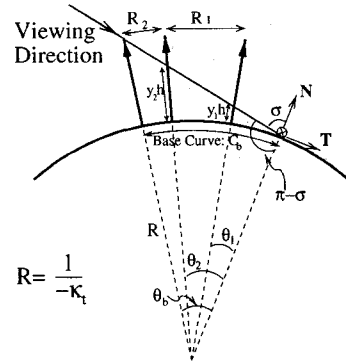


Figure 6: Viewing from one of the local principal curvature directions. The base curve is marked on the graph. The plane is the (\mathbf{T}, \mathbf{N}) plane.

in other words, the base curve lies completely on the (\mathbf{T}, \mathbf{N}) plane.

The (\mathbf{T}, \mathbf{N}) plane is shown in Figure 6. σ is the slant of the surface at the location where the viewing ray hits the surface. The local frame field is defined at that point. Let the principal curvature be $\kappa_t = -1/R$. The local curvature is assumed to be constant in the neighborhood of the point where the viewing ray hits the surface. The base curve C_b is an arc subtending an angle θ_b as marked in the figure. The length of C_b is $R\theta_b$. We can calculate θ_b using the sine rule:

$$\frac{R+h}{\sin(\pi-\sigma)} = \frac{R}{\sin(\sigma-\theta_b)}$$

Simplifying and substituting $R = -k_t^{-1}$:

$$\theta_b = \sigma - \text{asin}(\sin \sigma (1 - h k_t)^{-1})$$

The length of the base curve is thus $\theta_b / (-k_t)$. Similarly, for an element on the base curve:

$$\theta_i = \sigma - \text{asin}(\sin \sigma (1 - y_i h k_t)^{-1})$$

As in the planar case, whether we can see the middle element in Figure 6 depends totally on the region R_2 . R_2 is a *tube* of width $2r$ and length $(\theta_b - \theta_2) / (-\kappa_t)$. Using a poisson model, the probability of no occlusion is $P_{NO} = \exp(-\lambda A(R_2))$:

$$P_{NO} = \exp(-2r\lambda(\theta_b - \theta_2) / (-k_t)) \quad (7)$$

By taking the derivative with respect to κ_t , we can show that P_{NO} increases as $|\kappa_t|$ increases, ie. as curvature increases, elements are turning away from the line of sight and so the probability of no occlusion increases. It can also be shown that when $\kappa_t \rightarrow 0$, we get back Equation 1 for the planar case.

Suppose the elements are painted yellow in the range $(y_1 h, y_2 h)$, the probability of seeing yellow in the pixel along the viewing direction is then given by:

$$\begin{aligned} \Pr(\text{yellow}) &= \Pr(N(R_2) = 0) \cdot \Pr(N(R_1) > 0) \\ &= e^{-\lambda A(R_2)} \cdot (1 - e^{-\lambda A(R_1)}) \\ &= e^{-2\lambda r \frac{\theta_b - \theta_2}{-\kappa_t}} - e^{-2\lambda r \frac{\theta_b - \theta_1}{-\kappa_t}} \end{aligned} \quad (8)$$

where $A(R_2) = 2r(\theta_b - \theta_2)/(-\kappa_t)$ and $A(R_1) = 2r(\theta_2 - \theta_1)/(-\kappa_t)$. Plots of these curves for values of y_i discussed in Section 4.2 are shown in Figure 10(b).

5.1.2 Generic Viewing Directions

We now consider the case $\tau \neq 0$. This means that we are not looking at the surface from one of the two principal curvature directions. We call this the generic viewing condition. Recall that a local frame field $(\mathbf{T}, \mathbf{B}, \mathbf{N})$ is defined at the point where the viewing ray intersects the surface (see Figure 5). Let the slant at that point be σ . As in the previous two cases, we want to find the base curve C_b , which specifies the locations of the bases of the elements which intersects the viewing ray. In the generic viewing condition, surface normals lying outside the (\mathbf{T}, \mathbf{N}) plane can intersect the viewing ray, so C_b does not necessarily lie completely on the (\mathbf{T}, \mathbf{N}) plane.

Recall that the texture elements are small compared to the global structure of the surface, ie. $|\kappa h| \ll 1$, where κ is any one of the curvature parameters $(\kappa_t, \kappa_b, \tau)$. Therefore, in the following analysis, terms of the order $O((\kappa h)^2)$ or higher are ignored.

We now proceed to determine the base curve for curved surfaces. Let us first find where the base of each potentially occluding element lies. Due to local curvature of the surface, an element based at $(\Delta t, \Delta b)$ will not lie on the tangent plane (\mathbf{T}, \mathbf{B}) . The distance from the tangent plane can be calculated from the normal section. Rewrite the displacement $\mathbf{v} = (\Delta t, \Delta b)$ in polar form: $(\Delta v, \theta)$. The normal curvature along \mathbf{v} is:

$$\begin{aligned} \kappa_\theta &= \begin{bmatrix} \cos \theta & \sin \theta \end{bmatrix} \begin{bmatrix} \kappa_t & \tau \\ \tau & \kappa_b \end{bmatrix} \begin{bmatrix} \cos \theta \\ \sin \theta \end{bmatrix} \\ &= \kappa_t \cos^2 \theta + 2\tau \sin \theta \cos \theta + \kappa_b \sin^2 \theta \end{aligned}$$

The situation is shown in Figure 7. The angle α subtended by Δv can be written as $\alpha = \Delta v/R = -\kappa_\theta \Delta v$. The distance below the tangent plane is then given by:

$$\begin{aligned} \Delta h &= R - R \cos \alpha \\ &= (-\kappa_\theta^{-1}) - (-\kappa_\theta^{-1})(1 - \alpha^2/2) \\ &= -\Delta v^2 \kappa_\theta / 2 \\ &= (-\kappa_t \Delta t^2 - 2\tau \Delta t \Delta b - \kappa_b \Delta b^2) / 2 \end{aligned} \quad (9)$$

The direction of this element is given by the surface normal at $(\Delta t, \Delta b)$ and is $\mathbf{N} + \nabla_{\mathbf{v}} \mathbf{N} =$

$$\mathbf{N} + \delta_t \mathbf{T} + \delta_b \mathbf{B} \quad (10)$$

We can write it as $[\delta_t, \delta_b, 1]$ with respect to the $(\mathbf{T}, \mathbf{B}, \mathbf{N})$ frame field. We now have a parametrization along the length of the element:

$$(\Delta t, \Delta b, -\Delta h) + yh[\delta_t, \delta_b, 1] \quad (11)$$

where yh is the distance from the base of the element, ranging from 0 to h . (Compare with Sections 4.1 and 5.1.1.)

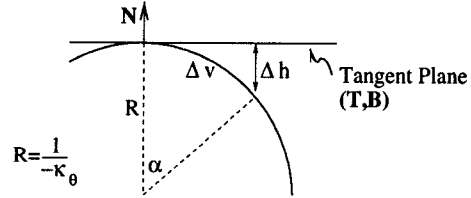


Figure 7: Due to the local curvature, an element at $(\Delta t, \Delta b)$ does not lie on the tangent plane. The distance from the tangent plane is given by Δh .

From Figure 5, the element intersects the (\mathbf{T}, \mathbf{N}) plane when

$$\Delta b + yh\delta_b = 0 \quad (12)$$

As a side note, Equation 12 tells us the order of $\kappa \Delta b$. Multiplying both sides by a curvature parameter κ , we have:

$$\kappa \Delta b + \kappa h(-\Delta t \tau - \Delta b \kappa_b) y = 0 \quad (13)$$

$(-\Delta t \tau - \Delta b \kappa_b)$ is of order $O(\kappa h)$, this implies $\kappa \Delta b$ is of order $O((\kappa h)^2)$. What this means physically is that though the base curve does not lie exactly on the (\mathbf{T}, \mathbf{N}) plane, the deviation is small.

We now proceed to compute the intersection point between the element located at $(\Delta t, \Delta b, -\Delta h)$ and the (\mathbf{T}, \mathbf{N}) plane. Let the intersection point be $(\Delta t_i, \Delta h_i)$. Using Equations 11 and 12, we have

$$yh = \frac{\Delta b}{\Delta t \tau + \Delta b \kappa_b} \quad (14)$$

$$\Delta t_i = \Delta t + yh \delta_t \quad (15)$$

$$\Delta h_i = -\Delta h + yh \quad (16)$$

We can simplify Δh to first order in κh by taking into account that $\kappa \Delta b = O((\kappa h)^2)$. The second and third terms in Equation 9: $(\tau \Delta b) \Delta t$ and $(\kappa_b \Delta b) \Delta b$ are both of order $O((\kappa h)^2)$, while the first term: $\kappa_t \Delta t^2$ is of first order in κh . Therefore, we can simplify Δh to:

$$\Delta h = (-\kappa_t \Delta t^2) / 2 \quad (17)$$

Equations 15 and 16 can then be written as:

$$\Delta t_i = \Delta t - \Delta b (\Delta t \kappa_t + \Delta b \tau) (\Delta t \tau + \Delta b \kappa_b)^{-1} \quad (18)$$

$$\Delta h_i = \kappa_t \Delta t^2 / 2 + \Delta b (\Delta t \tau + \Delta b \kappa_b)^{-1} \quad (19)$$

We now know the location where the element based at $(\Delta t, \Delta b, -\Delta h)$ intersects the (\mathbf{T}, \mathbf{N}) plane. As shown in Figure 8, the intersection point will be along the viewing ray if

$$-\Delta t_i = \Delta h_i \tan \sigma \quad (20)$$

Expanding and ignoring terms with order $O((\kappa h)^2)$ or higher, Equation 20 can be written as a quadratic equation in Δt and Δb :

$$\tan \sigma \Delta b + \tau \Delta t^2 = 0 \quad (21)$$

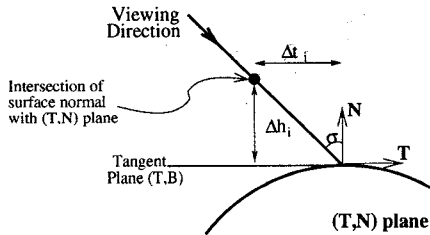


Figure 8: The surface normal is rotated so that it intersects the (\mathbf{T}, \mathbf{N}) plane at the point $(\Delta t_i, \Delta h_i)$. This intersection point is along the viewing ray if Equation 20 are satisfied.

When $\tau = 0$, Equation 21 simplifies to $\Delta b = 0$. This says, under principal viewing conditions, we only need to care about surface normals on the \mathbf{T} axis, which is exactly our observation in Section 5.1.1.

Combining Equation 21 with the constraint on the height of the elements ($yh \leq h$):

$$\frac{\Delta b}{\Delta t\tau + \Delta b\kappa_b} \leq h \quad (22)$$

we can specify the points on the base curve. It is shown in Figure 9. The base curve consists of all the points $(\Delta t, \Delta b, -\Delta h)$ where Δt and Δb satisfy Equation 21 and the constraint in Equation 22; Δh is given by Equation 17. Taking into account the radius r of the elements, we have the base region R_b , which is the tube of width $2r$ around the base curve. One point to notice is that each point on the base curve completely specifies the intersection point between the surface normal and the viewing ray by Equation 14. Thus, occlusion probabilities or probabilities of seeing a particular color along a viewing direction are completely determined by the base curve.

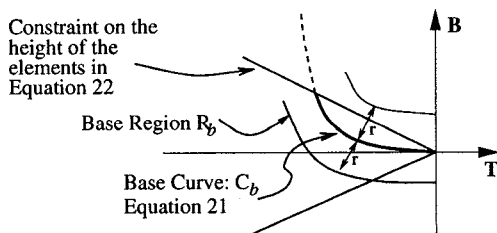


Figure 9: The base curve C_b for a curved surface in generic viewing condition. The base region R_b is a tube of width $2r$ around the base curve.

6 Experiments

In this section, we investigate how good our model is and verify some of the approximations that we made. We first compare our predictions on the probability of seeing a particular color to the empirical values in synthetic images for both planar and spherical surfaces. The predicted values are shown as the solid curves in Figures 10(a) and (b) for planar and

spherical surfaces respectively. In the synthetic images, the elements are modeled as cylinders with the bottom 3/4 of the stem green and the upper 1/4 of the stem and the top yellow, same as those discussed in Section 4.2. The height of the element h is 20 and the radius r is 1. The locations of the elements are realizations of a hard-core model with inhibition radius 1 on a plane and on a sphere. The intensity of the process λ is 0.01. We generated 60 images for each of the two surface types. Since we know the actual surface geometry, we can compute the slant of the surface at every pixel on the image. The slant is divided into 36 bins evenly distributed from 0 to $\pi/2$. Each set of images is divided into 6 groups. The average probability for each color is calculated as a function of slant for each group. The mean over the 6 groups are plotted as the crosses in Figure 10. The standard deviations over the 6 groups are used as an error estimate of the probabilities. The error bars in the plots are the 2σ points. Notice that the predicted and the measured values agree very well even though we assume a poisson model in our predictions while the images are generated using a hard-core model. $\lambda\pi r^2 = 0.031$ is small, which explains why the poisson model is a good enough approximation.

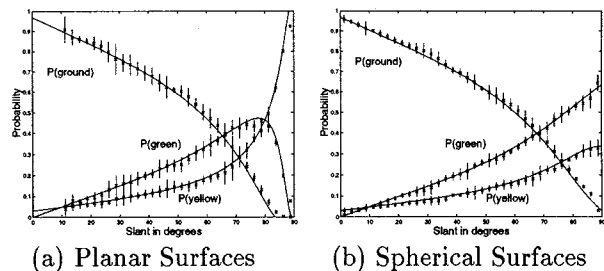


Figure 10: Probabilities of seeing a particular color vs slant. $\lambda hr = 0.2$. The curvature $\kappa_t = 0.002$ for the spherical surface. The solid curves are the predicted values by our model. The “x”s mark the mean of the empirical probabilities obtained from 60 synthetic images. The error bars indicate 2σ points.

The second experiment we performed was aimed to investigate how good our model is for real scenes. We considered the region in the white box in the “field of yellow flowers” image shown in Figure 11. Simple color quantization is performed to extract the yellow pixels and they are shown on the right in Figure 11.

We make the simplifying assumption that we are looking at the ground plane. However, the slant of the ground is unknown. The elements are modeled as cylinders with the upper 1/4 of the stem painted yellow as discussed in Section 4.2³. The free parameter of the model is λhr which measures the crowdedness of the elements.

Given an estimate of the slant at the center of the image σ_0 and an estimate for λhr , we can compute the

³We ignore the top of the cylinder because its effect on our model is very small (Equation 4).

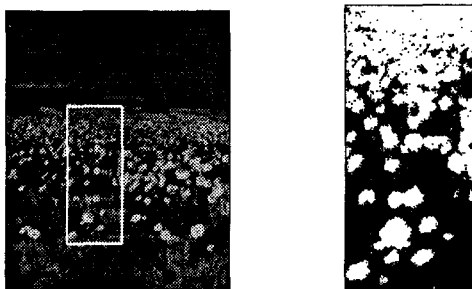


Figure 11: A field of yellow flowers. We consider the region marked by the red box on the left image. The image on the right shows the yellow pixels in the red box using simple color quantization.

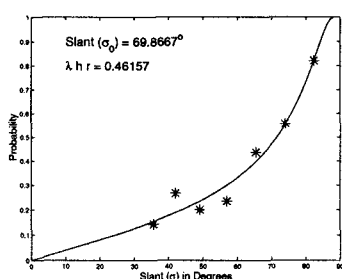


Figure 12: The solid curve is the probability of seeing yellow using our model. The “*”s are values computed in the image. The parameters of our model are estimated using nonlinear least square minimization. The “crowdedness” parameter obtained is: $\lambda h r = 0.4616$ and the slant in the center of the image is estimated to be 69.87° .

empirical probability of seeing yellow from the image as a function of slant. The mean square difference between the measured values and the values predicted by our model is the error. Minimization of this error is a standard nonlinear least square problem. The result of the minimization is: $\lambda h r = 0.4616$ and $\sigma_0 = 69.87^\circ$. These values are quite insensitive to the choice of initial values for the minimization. Using these parameters, the predicted curve is shown as the solid line in Figure 12. The probabilities of yellow computed from the image are shown as the “*”s.

7 Conclusions and Discussions

We have presented a model for a special class of 3D textures, *perpendicular* textures. 3D textures have been largely ignored in the analytical study of texture in both computer vision and graphics. In this paper, we have presented results relating the occlusion properties of the surface in the scene and the image. Experiments with synthetic images have verified some of the approximations for the calculation of the different probabilities. A real image is used to illustrate the applicability to real scenes. Occlusion, which is usually being treated as an error, can now be used as a cue to infer surface shape.

In the present work, the results are derived for one model — constant height elements in a homogeneous poisson field. However, for many real world objects, other models will be more appropriate, e.g. hard core models with inhibition radius r , elements with non-constant heights or elements not perpendicular to the surface. All these are straight forward generalizations of our present model. Closed form formulae for the different probabilities are difficult to obtain, but numerical solutions are easy enough. Indeed, we have computed numerical solutions for both hard-core models and gaussianly distributed height models. For random height distributions, occlusion effects can be well approximated using elements with constant height equal to the mean of the distribution. Details of these experiments are skipped in this paper due to space constraints.

Combining the geometric part we presented in this paper together with the photometric part of the problem is an interesting issue. If we ignore mutual illumination and inter-reflection, whether an element will be illuminated by a point light source is just the same as the visibility probability we have studied. The observer will become the light source and the probability that we can see the element is equivalent to the probability that the element is under illumination. However, if we include other effects such as inter-reflection, the problem is much more complicated. Once this problem is solved, we could use our model for fast rendering of objects covered with hair or fur.

Acknowledgement

This work was supported by the Digital Library Grant IRI-9411334 and a Berkeley Fellowship.

References

- [1] A. Blake and C. Marinos. “Shape from texture: estimation, isotropy and moments”. *Artificial Intelligence*, 45, 1990.
- [2] D. Blostein and N. Ahuja. Shape from texture: Integrating texture-element extraction and surface estimation. *IEEE Trans. Pattern Anal. Mach. Intell.*, 11(12), 1989.
- [3] J.D. Foley, A. van Dam, S.K. Feiner, and J.F. Hughes. “Computer graphics, principles and practice”. Addison-Wesley, 1990.
- [4] J. Gårding. “Shape from texture for smooth curved surface in perspective projection”. *Journal of Mathematical Imaging and Vision*, 2(4):327–50, Dec. 1992.
- [5] J.J. Gibson. “The perception of the visual world”. Houghton Mifflin, Boston, 1950.
- [6] J.T. Kajiya and T.L. Kay. “Rendering fur with three dimensional textures”. In *Computer Graphics (SIGGRAPH '89 Proceedings)*, volume 23, pages 271–280, July 1989.
- [7] J.J. Koenderink and A.J. van Doorn. “Illuminance texture due to surface mesostructure”. *J. Opt. Soc. Am. A*, 13:452–463, March 1996.
- [8] J. Malik and R. Rosenholtz. “Computing local surface orientation and shape from texture for curved surfaces”. *Int. J. of Computer Vision*, 23(2), June 1997.
- [9] B.D. Ripley. “Modelling Spatial Patterns”. *J. Royal Statistical Society B*, 39(2):172–192, 1977.
- [10] D. Stoyan and H. Stoyan. “Fractals, random shapes and point fields”. Wiley, 1994.